Accepted Manuscript

Title: Change of the yield stress in roll formed ERW pipes considering the Bauschinger effect

Authors: Joonmin Lee, Dongwook Kim, Luca Quagliato, Soochang Kang, Naksoo Kim

PII: S0924-0136(17)30022-5
DOI: http://dx.doi.org/doi:10.1016/j.jmatprotec.2017.01.022
Reference: PROTEC 15097

To appear in: *Journal of Materials Processing Technology*

Received date: 29-3-2016
Revised date: 18-1-2017
Accepted date: 21-1-2017

Please cite this article as: Lee, Joonmin, Kim, Dongwook, Quagliato, Luca, Kang, Soochang, Kim, Naksoo, Change of the yield stress in roll formed ERW pipes considering the Bauschinger effect.Journal of Materials Processing Technology http://dx.doi.org/10.1016/j.jmatprotec.2017.01.022

This is a PDF file of an unedited manuscript that has been accepted for publication. As a service to our customers we are providing this early version of the manuscript. The manuscript will undergo copyediting, typesetting, and review of the resulting proof before it is published in its final form. Please note that during the production process errors may be discovered which could affect the content, and all legal disclaimers that apply to the journal pertain.

ACCEPTED MANUSCRIPT

Change of the yield stress in roll formed ERW pipes considering the Bauschinger effect

Joonmin Lee[1], Dongwook Kim[1], Luca Quagliato[2], Soochang Kang[3] and Naksoo Kim [1*]

[1]Sogang University, Department of Mechanical Engineering, Seoul, 121-742, Republic of Korea

[2]Padua University, Department of Management and Engineering, Vicenza, 36100, Italy

[3]Global R&D Center, POSCO, Incheon 21985, Republic of Korea

*Corresponding author/ Phone: +82 2-712-0799, Fax: +82 2-712-0799, E-mail address: nskim@sogang.ac.kr

ABSTRACT

ERW pipes formed with the roll forming process show a yield stress distribution along the circumferential direction and their quality is strongly influenced by the magnitude and by the distributions of the yield stress. In addition to that, strips are subjected to cyclic loading during roll forming process.

Since ERW pipes are firstly roll formed, welded and then sized, in order to develop an enhanced predicting method for the calculation of the ERW pipe yield stress, the same process flow has been also applied to authors' numerical simulations.

The Yoshida-Uemori kinematic hardening model has been applied considering several subdivision of the strain range, and different parameters, aiming to find the best correlation between the estimated Bauschinger effect and the one measured in the relevant cyclic loading experiment.

The comparisons between estimated and experimentally-measured values of the thickness distribution, and of the locally-measured yield stress, prove both reliability and accuracy of the adopted process chain analysis.

The growth of the sizing effect ratio has shown to cause the increase of the yield stress, which becomes more uniform along the circumferential direction.

KEYWORDS: ERW pipe, roll forming, Sizing effect, Yield stress distribution, Bauschinger effect, Modified Yoshida-Uemori model, Process chain analysis

ACCEPTED MANUSCRIPT

1. INTRODUCTION

The continuous growth tendency in the demand for energy power is directly linked to the increasing need for oil and gas transportation pipes, such as OCTG (Oil country tubular goods) and Line pipes. The ERW (Electric Resistance Welding) roll forming process is widely utilized for the production of steel pipes and is normally composed of six different stations: uncoiling, leveling, roll forming, welding, sizing, and straightening, as shown in Fig. 1. With the rotation of the rollers, the strip deforms continuously to a circular cross-shaped pipe. Since the grade of change in the material yield stress is also caused by the fabrication process, the same strip of material has shown different behaviors if utilized by different steel pipes companies.

In particular, it is not easy to predict the yield stress after the production, since tension and compression stresses are repeatedly applied on the strip. Multiple tensile and compression repetitions cause the yield point of the material to change several times due to Bauschinger effect and make the yield stress to be completely different from that of the initial plate. In addition to that, every pipe is manufactured starting from different strip, which makes the yield stress of the final product to be influenced by initial strip mechanical properties and welding process, as well it varies along the circumferential direction of the pipe.

Due to the intrinsic difficulty in understanding the change mechanism of the mechanical properties of the pipe, the know-how of the production operator is a major factor influencing the mechanical properties. If a trial-and-error procedure is applied in order to determine the best process configurations, it shall result in being a high time and expensive procedure. For this reason, the understanding of the phenomenon that influence the variation of the yield stress is a key point to quickly and successfully set up the production process, avoiding trial-and-error procedures in favor of a more systematic and capable strategy.

In this paper, the work hardening state of the material is studied utilizing numerical analysis technique, aiming to determine possible changes in its yield stress.

In the past, much effort has been spent by several authors trying to solve this problem. Kim et al.(2003) studied the edge shape of strip before welding, in order to determine the weld quality of ERW pipe, discovering that the optimized edge shape, which ensures a good weld ability, can be obtained by pre-machining the strip edge.

Cha et al.(2013), through FE simulations, studied twisting and bowing defects on roll formed products made of high strength steel using V-channel roll forming process, confirming the possibility of designing edges and webs those can minimize these two defects.

Wiebenga et al.(2013) analyzed the phenomenon of longitudinal bow and springback defects dependent to roll gap using a ANOVA (Analysis Of Variance) for U-channel roll forming process. Thehrani et al.(2006) studied the edge buckling and longitudinal strain of the web during the U-channel roll forming process. Park et al.(2014), by studying the cross-sectional shapes and the longitudinal strain by using the simplified ICF(Incremental Counter forming), confirmed that the longitudinal strain occur differently according to the process conditions. Kasaei et al.(2014, 2014) conducted a study on the edge buckling, the longitudinal strain, and the edge gap controlled by process parameter using cage roll forming process and flexible roll forming FE model. Zou et al.(2015), (2016) Ren et al.(2015), and Herynk et al.(2007) studied UOE forming(U-forming, O-forming, Expansion) based on the numerical model. Their results shown that the O-forming gap is influenced by the process parameters and an algorithm was developed to obtain the distribution and history of the yield stress

ACCEPTED MANUSCRIPT

during the process. They showed that U-forming radius is the most important factor in C- and U-forming stages to determine O-forming gap, and the opening gap width increases with increasing of compression ratio in the O-forming stage. Gehring et al.(2007) performed an analysis on base of a statistical design approach in order to identify the effects and interactions of different parameters on profile properties. The parameters included in the analysis are the roll diameter, the rolling speed, the sheet thickness, friction between the tools and the sheet and the strain hardening behavior of the sheet material.

During roll forming processes, material are subjected to fast repetition of tension and compression effect which make the so-called Bauschinger effect and working hardening phenomenon appear. Many studies on the hardening models capable of accurately simulating this phenomenon have been made.

Prager (1956) proposed a kinematic hardening model able to describe the Bauschinger effect. The yield surface in Prager's model is assumed to move in a direction perpendicular to the surface during loading. Ziegler (1959) modified the Prager's assumption that the yielding surface move radially by a vector (**s-a**), where **s** and **a** are the stress tensor and the back stress, respectively. Yin et al.(2012) used NKH (Nonlinear kinematic hardening) model to have a best fitting of the cyclic-load test results, applying the model to a forming process in order to simulate the springback effect. The results showed how a NKH model is not able to predict the compression behavior and estimate the Bauschinger effect.

Yoshida and Uemori (2002, 2013) proposed a yield surface with an additional bounding surface to describe the Bauschinger effect. The so-called Y-U (Yoshida-Uemori) model, which includes many model constants, has been applied to various materials and utilized in several different applications, and was expected to describe the actual Bauschinger behavior quite well. Jia (2014) used the robust integration algorithm in order to simplify the Y-U model and tried to find the feasibility of the numerical model for the cyclic load test. Instead, Ghaei (2015) and Sumikawa (2014) demonstrated, with experiments and numerical models, that the Y-U model describes the Bauschinger effect very well and can predicts the springback precisely in the simulation. Jia and Kuwamura (2015) proposed a combined method of a damage model and the Y-U model for the accurate prediction of ductile fracture in conditions of large deformation. Silvestre et al.(2015) used a mixed isotropic-kinematic hardening model combined with Chaboche model and Lemaitre model to apply and check the feasibility for cyclic load test of various materials such as mild steel, stainless steel, DP (Dual Phase) steel, and TRIP (Transformation-induced plasticity) steel. The other studies to simulate the Bauschinger effect and the working hardening behavior are homogeneous yield function-based anisotropic hardening (HAH) model proposed by Barlat et al.(2011), non-saturating kinematic Swift (NSK) model proposed by Xiao et al.(2012), and Barcelona plastic damage model proposed by Barbu et al.(2015).

Studies on the mechanical properties of roll-formed pipes from the strip have been conducted, as follows. Han et al.(2012) found that the increase of Vickers hardness of the X80 steel pipe after roll forming process resulted from the pre-strain. They confirmed that the magnitude and the distribution of the yield stress in the thickness direction varied depending on the level of pre-strain.

Son et al.(2013) also confirmed that the yield stress of pipe in the thickness direction is reduced inside and increased outside of the pipe by 1.5% to 1.25%, in accordance with the pre-strain effect. Zeinoddini et al.(2015) evaluated the residual stress using the denting axial compression test. Kraft and Jamison (2012) found that the flow stress in the longitudinal direction of pipe was higher than that in the circumferential direction after tensile

ACCEPTED MANUSCRIPT

tests with specimens at each direction. Even they also confirmed that the magnitude of flow stress with the same material showed differences depending on diameter and thickness. Previous researches have been focused on the phenomenological observation of pipe after roll forming process.

Since it is not easy to include the history of the longitudinal elongation and the increase of thickness the during roll forming process in a complicated hardening model, an analysis based on an efficient and accurate numerical model is required to predict the change of the yield stress.

Due to the multiple tension and compression applied to the strip, it is not easy to include the history of the longitudinal elongation and of the thickness increase during a forming process that creates a flower pattern through at least 20 rolls or more. An analysis based on an efficient and accurate numerical model is required to predict the change of the yield stress.

In section 2, a modified Yoshida-Uemori (MYU) model, which can be configured to precisely express the hardening of the material, is proposed. Section 3 describes the methods and procedures for the material parameters used in the model. Section 4 describes the process chain analysis and explains how the numerical model operates in the roll forming process and sizing process.

The numerical simulation results were validated by comparison with the calculated results with the measurements for both the circumferential length and the thickness, at various locations along the circumference. In section 5, the results of the prediction of the yield stress of the pipe, after the process chain, are shown and commented. Comments and consideration are also drawn in case of differences between computed and measured yield stress values. The sizing ratio, defined as the amount of thickness calibration during the sizing phase, is also an important parameter and its influence on the yield stress was investigated and the relevant results are presented in this paper.

2. The constitutive model

The strip experiences a repetitive deformation of tension and compression during roll forming process then, in order to properly set-up the simulation, a hardening model able to accurately describe the Bauschinger effect is required.

The Y-U model consists of the yield surface with the kinematical motion based on the two-surface model in the bounding surface(Yoshida et al. 2002). The yield surface represents the kinematic hardening, while the bounding surface is configured to express a mixed isotropic-kinematic hardening. The kinematic hardening or the movement of the yield surface due to the pre-strain describes the Bauschinger effect, while the bounding surface compensates for the global working hardening to describe permanent softening.

The yield function *f* and the bounding surface *F*, based on the von Mises yield function, are expressed in eqns. (2.1) and (2.2), respectively.

$$f = \sqrt{\frac{3}{2}(\boldsymbol{\sigma} - \boldsymbol{\alpha})} - \sigma_{Y,i} = 0 \tag{2.1}$$

$$F = \sqrt{\frac{3}{2}(\boldsymbol{\sigma} - \boldsymbol{\beta})} - (B_i + R) = 0 \tag{2.2}$$

ACCEPTED MANUSCRIPT

, where $\boldsymbol{\sigma}$ and $\boldsymbol{\alpha}$ are the Cauchy stress tensor and the back stress tensor, respectively. $\sigma_{Y,i}$ is the initial yield stress, B_i and R are the initial size and isotropic hardening of the bounding surface, respectively. $\boldsymbol{\beta}$ represents the motion of the bounding surface.

As previously stated, the kinematic hardening of the yield stress describes the Bauschinger effect and the mixed isotropic-kinematic hardening of bounding surface represents the global work hardening. The relationship between the yield surface and the bounding surface can be established considering the relative kinematic motion of the yield surface, with respect to the bounding surface, and is expressed by the parameter $\boldsymbol{\theta}$, eqn. (2.3).

$$\boldsymbol{\theta} = \boldsymbol{\alpha} - \boldsymbol{\beta} \tag{2.3}$$

The evolution of the three back stress tensors are defined as

$$d\boldsymbol{\alpha} = d\boldsymbol{\beta} + d\boldsymbol{\theta} \tag{2.4}$$

$$d\boldsymbol{\beta} = m_i \left[\frac{b_i}{\sigma_{Y,i}} (\boldsymbol{\sigma} - \boldsymbol{\alpha}) - \boldsymbol{\beta} \right] d\bar{\varepsilon}^p \tag{2.5}$$

$$d\boldsymbol{\theta} = C \left[\frac{b_i}{\sigma_{Y,i}} (\boldsymbol{\sigma} - \boldsymbol{\alpha}) - \sqrt{\frac{a}{\bar{\boldsymbol{\theta}}}} \boldsymbol{\theta} \right] d\bar{\varepsilon}^p \tag{2.6}$$

where $d\bar{\varepsilon}^p$ is the equivalent plastic strain, m_i, b_i, C are model parameters whereas $\bar{\theta}$ is the equivalent value of θ. The parameter a in eqn.(2.6) is defined as follows.

$$a = B_i + R - \sigma_{Y,i} \tag{2.7}$$

R is the kinematic part of the bounding surface and it is defined as

$$R = R_{sat,i}(1 - e^{-m_i \bar{\varepsilon}^p}) + h\bar{\varepsilon}^p \tag{2.8}$$

where $R_{sat,i}$ stands for the saturated value of the isotropic hardening stress, and where m_i and h_i are model parameters.

Yoshida et al.(2002) shown that the two-surface kinematic hardening model shown in eqns. (2.1) - (2.8) shows limitations in predicting the yield stress, especially during compression after tension. Therefore, in this paper, in order to precisely calculate the flow stress, a segment-wise material properties $\sigma_{Y,i}, B_i, R_{sat,i}, b_i, m_i$ approach for the Yoshida-Uemori model parameters, dependent on the equivalent plastic strain $\bar{\varepsilon}^p$, is proposed.

ACCEPTED MANUSCRIPT

$$\begin{cases} \sigma_{Y,1}, B_1, R_{sat,1}, b_1, m_1 & \text{if} \quad \bar{\varepsilon}^p \le \bar{\varepsilon}_1^p \\ \sigma_{Y,2}, B_2, R_{sat,2}, b_2, m_2 & \text{if} \quad \bar{\varepsilon}_1^p \le \bar{\varepsilon}^p \le \bar{\varepsilon}_2^p \\ \sigma_{Y,3}, B_3, R_{sat,3}, b_3, m_3 & \text{if} \quad \bar{\varepsilon}_2^p \le \bar{\varepsilon}^p \end{cases} \tag{2.9}$$

In the above strain segments, $\bar{\varepsilon}_1^p$ denotes the first maximum tensile plastic strain during the cyclic load test, while $\bar{\varepsilon}_2^p$ is the plastic strain at the first maximum compressive yielding after tension. Since it is not natural that parameters show any discontinuities to describe the flow stress, the linear interpolation parameters P_1, P_2, P_3 are considered in order to obtain values for η_1, η_2, η_3 which can be numerically utilized, as summarized in eqn. (2.10).

$$\begin{cases} \eta_1 = P_2 + (1-\delta_1)(P_1 - P_2), \\ \eta_2 = P_3 + (1-\delta_2)(P_2 - P_3), \\ \eta_3 = P_3 \end{cases} \tag{2.10}$$

, where δ_1, δ_2 are weighting factors that can linearly change η_1, η_2, η_3 according to the plastic strain $\bar{\varepsilon}^p$.

$$\delta_i = \frac{\bar{\varepsilon}^p}{\bar{\varepsilon}_i^p} \qquad (i = 1, 2) \tag{2.11}$$

After the plastic deformation of a material, it has been found that the elastic modulus decreases during unloading and it attains to a converged value after certain equivalent plastic strain (Yoshida et al. 2002) and (Morestin and Boivin 1996).

In the numerical model, the effect of equivalent plastic strain of Young's modulus, E_{ep} was taken into account using the following empirical equation (Yoshida et al. 2002).

$$E_{ep} = E_0 - (E_0 - E_a)[1 - \exp(-x_i \varepsilon^p)] \tag{2.12}$$

where E_0 and E_a stand for the elastic moduli at initial and infinitely large pre-strain stage, respectively, while x_i is a model parameter.

3. Model Parameters

The steel used in this study was an API (American Petroleum Institute) standards K55 with the material

ACCEPTED MANUSCRIPT

chemical compositions as summarized in Table 1. The material behavior has been measured in both a uniaxial tensile test and a cyclic load test. Fig. 3 shows the stress-strain curves of the specimen obtained from the test results. The Bauschinger effect causes a reduction of yield stress after the re-yielding compared with that of the initial stress.

The model parameters for material property have been determined in the order to match the behavior of the test results. All simulation was conducted with ABAQUS, while the constitutive model was applied in the calculation by supplying the user-defined subroutine VUMAT. The simple-element model with C3D8R type mesh as shown in Fig. 4 with the same conditions as in tensile test was applied in the simulation.
Several literature contributions in different metal forming areas, such as in: Zou et al.(2016) for the roll forming process, Tajyar et al.(2009) for the non-circular tube forming process, Cai et al.(2014) for the roll forming process, Yang et al.(2006) and Guo et al.(2006) for the ring rolling process, have shown that by utilizing the C3D8R (reduced-integration element), instead of the C3D8 (fully-integrated element) or C3D8I (incompatible-mode element), it is possible to obtain precise results with a considerable spare of time. Since in the analyzed process several consecutive complex plastic deformations are involved and being the C3D8 a fully-integrated element, whereas the C3D8R reduced-integration element, the utilization of the last one allows reducing the computational time thanks to a reduced number of integration points, while ensuring a precise calculation.

The true stress-strain curve was obtained by a cyclic load simulation using the simple-element model. The area of the difference E_{diff} has been defined denoting the discrepancy of the experimental results σ_{ex} and the analysis results σ_{sim} as expressed in equation (3.1). In order to systematically minimize E_{diff}, the PQRSM (Progressive Quadratic Response Surface Modeling) technique was used. PQRSM is a method of updating the Hessian matrix to produce a full quadratic response surface shape of the simulation based on a set of given design parameters. The aim is to minimize the object function within a variable range. By iterative calculation, confidence intervals can be reduced and ultimately accurate and reliable minimum values can be obtained.

$$E_{diff} = \frac{1}{N} \sum \left| \frac{\sigma_{ex} - \sigma_{sim}}{\sigma_{ex}} \right| \times 100 \tag{3.1}$$

As shown in Fig. 5, since the area of the difference is 2% or less, the numerical model was confirmed to have a good representation of the actual behavior. In addition, when using the MYU model, it was possible to obtain far more accurate results compared to the YU model. MYU model complements the limits of YU model by applying the variable section separately in the pipe process which undergoes complicated behavior and more precisely copies the behavior of the material. Calculated Parameters are summarized in Table 2.

4. Process chain analysis of ERW roll forming

ERW roll forming process is used to manufacture the uncoiled flat strip gradually into a pipe with circular

ACCEPTED MANUSCRIPT

cross section as the strip passes through several roll stands. It is to verify that ERW roll forming process simulation with the hardening model parameters obtained from the cyclic load test predicts the actual physical phenomena.

4.1 Numerical simulation of roll forming process

As concerns the numerical simulation of ERW roll forming process, input data of roll shape, roll rotation velocity, and distance between roll stands as used in the actual roll forming line have been considered. The simulation conditions and the geometry of the workpiece are reported in Table 3. Even though the mesh was constructed for the whole region of roll forming process-line, to give enough friction to the strip and limit the computational time, only region B was modeled with fine meshes, as shown in Fig. 6. Aiming to show the evolution of the forming process the position of the end of the strip, for each step, is reported in Table 4 where, the "stand number 0" means the initial state of the strip.

The strip during roll forming experiences deformation in the circumferential, thickness and longitudinal direction. Each material point at located in the circumference undergoes a specific stress-strain history. For a roll-formed pipe, the two circumferential locations (θ) of 90° and 180°, respectively, relative to the weld line, have been tracked in order to record the strain history, as shown in Fig. 7.

It is observed that the inner layer is the first to be interested by a tensile deformation while the outer layer undergoes a compression deformation; afterwards the patter is reversed. Moreover, also the repetitive loading-unloading phenomenon is observed while the strip passes through the stands.

Even though the magnitude of the yield stresses looks bounded, the deformation history pattern is much different if different circumferential positions are considered.

Before the welding process and after the completion of roll forming, only the circumference length can be measured hence, in order to confirm the accuracy of the simulation, the FE results have been compared with the those of the experiments, as illustrated in Table 5. The circumference lengths has been measured 10 times on different positions and averaged along the longitudinal direction. It can be stated that the process chain-analysis procedure is quite accurate to simulate the actual roll forming line since the discrepancy between simulation and experimental results is limited to a 0.4 mm range.

The inclusion of the HF-ERW (High Frequency Electric Resistance welding) welding process into the developed numerical model seemed not realistic considering the computation burden. Therefore, in order to take into account its effect on the process, the circumferential length has been reduced of 2mm in order to match with the reality (experiment).

4.2 Numerical simulation of Sizing process

The sizing operation is the process phase where outer diameter and roundness of pipe are controlled by applying compression on the outer surface, either with the upper and lower rollers or with the left and right rollers. Briefly, it refers to the sizing step to match the desired dimensions after the roll forming step, after welding is over. It will produce pipes of the required dimensions via the sizing process. The sizing process has

ACCEPTED MANUSCRIPT

been also studied in the process chain analysis. Considering the compression or the degree of sizing reduce the outer diameter of pipe, the following sizing effect ratio has been considered.

$$\text{Sizing effect ratio} = \frac{OD_{before} - OD_{after}}{OD_{before}} \times 100 \ (\%) \tag{4.1}$$

where OD_{before} and OD_{after} are pipe diameters before and after sizing process, respectively.

Sizing effect ratio is a process condition generally determined by know-hows of operators but, since a change to the material itself according to the sizing effect ratio is unclear, it is used primarily in regulating the size of the outer diameter. The sizing effect ratio in the actual roll forming line has been measured to be about 0.2% as shown in Fig. 9(a). The simulation results for the case of 0.2% are obtained as shown in Fig. 8. The thickness at eight different locations is computed and compared with measurements, obtained using a micrometer as shown in Fig.9(b). The difference between the averaged measured value and the calculated value is found to be about 0.02mm. As it can be seen from both measurement and simulation results, the thickness does clearly increase after roll forming process but, the amount of growth different from position to position, since the different deformation history that characterize different positions.

5. Material test of roll formed pipe

5.1 Tensile test and simulation

The simulation results was compared, for cross verification, with those of tensile test, in order to ensure the reliability of the implementation. Tensile specimens have been selected in the longitudinal or rolling direction according to ASTM E8 standards of API 5L, at two pipe's location-4 and 8, respectively, as shown in Fig 10. By applying the calculated thickness, the plastic strain tensor, and the back stress tensor obtained from the simulation of sizing process, a simulation of tensile test has been performed.

Although, in general, a flow stress model is used to represent numerically a stress-strain curve obtained from the tensile test results, the yield stress calculated from a certain flow stress model may be different from those calculated from other flow stress models, which lowers the reliability of the yield stress prediction. This is caused by the fitting operation of the tensile test data, which is focused on the overall plastic strain range while the yield stress is sensitive only to the elastic-plastic boundary or very small plastic strain range.

In the present research work, by using the equation (5.1), the flow stress model is constrained to contain the measured yield stress; the equation parameters are determined to fit with the measured yield stress and the stress-strain curve in the range of strain 0.1 (considering that the tensile test has been performed twice). $R_{0.2\%}$, defined in eqn. (5.1), is the kinematic part of the bounding surface and represents the flow stress in the Yoshida-Uemori model.

$$R_{0.2\%} = 143(1 - e^{-87\bar{\varepsilon}^p}) + 0.35\bar{\varepsilon}^p \tag{5.1}$$

ACCEPTED MANUSCRIPT

Fig.11 shows the simulated and the measured load-stroke curves at two different locations after tensile tests, and the differences are particularly evident after the UTS (Ultimate tensile strength) point. The discrepancy is also evident if the load-stroke curve is converted into engineering stress – engineering strain curve, as shown in Fig.12. By regarding the proof stress of 0.2% offset of elastic line as the yield stress, it can be seen that the differences between the experiments and the computation values are 1MPa at the location #4 and 2 MPa at the location #8, respectively, as shown in Fig. 12. This last comparison allows stating that the proposed method is reliable in predicting the yield stress of the material in different position of the strip.

5.2 Effect of the sizing effect ratio on the yield stress

Using the previously described procedure, it is possible to calculate the yield stresses of a roll-formed pipe with different process parameter, especially varying sizing effect ratio, which can be controlled by changing the roll gap in the simulation, as it happens in the real production line.

Four different sizing effect ratios of 0.2, 1, 1.5, and 2.5%, which are usually performed in industry, were applied to the sizing process. Fig.13 exhibits an averaged diameter and thickness according to these ratios. The averaged thickness increases linearly while the averaged diameter decreases as the sizing effect ratio increases. This fact shows that it is possible to adjust the geometry of the pipe through a sizing process.

The distribution of the yield stress along the circumferential direction by using the method described in section 5.1 is shown in Fig.14. Due to work hardening, the overall increasing trend of the yield stress appeared. For example, the yield stress of 586MPa at the location #1 showed 10% increase over the initial one. The local-based deviation in the yield stress up to approximately 45MPa along the circumferential direction occurs because of the different deformation history.

It is notable that the high yield stresses at the locations #1, #2, and #3 is to be attributed to the initial excessive deformation during the early stage of W-bending process as shown in Fig.15.

6. Conclusions

In this paper, a numerical simulation model for the ERW roll forming process, aiming to predict the change in the yield stress of roll-formed ERW pipe, has been presented. Moreover, by using the segment-wise model parameters, a modified Y-U model has been derived in order to precisely describe the kinematic work hardening behavior of the strip. The proposed modified Y-U model has shown to overcome the limitation of the original Y-U model in the prediction of the yield stress in case of cyclic loading.

We used the M - Y - U model which can express the reduction of yield stress and the Bauschinger effect during re - yielding, and more precisely replicated the behavior of the material. This allowed the actual simulation analysis to more accurately reflect the actual situation

A process chain analysis has been applied to roll forming, welding, and sizing process in sequence. The procedure showed enough reliability after two cross verifications and comparisons between simulations and

ACCEPTED MANUSCRIPT

experiments results.

As concerns to the change of the yield stress of pipe compared with the strip, it can be concluded that the magnitude increases as the sizing effect-ratio increases, while the difference along the circumferential direction reduces.

It must be taken into account that the present study neglected the anisotropy of the strip, which may affect the yield stress. Finally, in terms of future works, the API test conditions of tensile test in the circumferential direction after flattening may be simulated with similar numerical procedures.

Reference

[1] Naksoo Kim., Byungseok Kang., Seungyoon Lee., 2003. Prediction and design of edge shape of initial strip for thick tube roll forming using finite element method. Journal of Materials Processing Technology. 142. 479-486.

[2] Wan-gi Cha., Naksoo Kim., 2013. Study on Twisting and Bowing of Roll Formed Products Made of High Strength Steel. International Journal Of Precision Engineering And Manufacturing. Vol. 14, No. 9. 1527-1533.

[3] J.H.Wiebengaa., M.Weiss., B.Rolfe., A.H.Van Den Boogaard., 2013. Product defect compensation by robust optimization of a cold roll forming process. Journal of Materials Processing Technology. 213. 978– 986.

[4] M.Salmani Tehrani., P.Hartley., H.Moslemi Naeini., H.Khademizadeh., 2006. Localised edge buckling in cold roll-forming of symmetric channel section. Advanced Materials Research. 44. 184-196.

[5] Jong-Cheol Park., Dong-YolYang., MyungHwanCha., DonGun Kim., Jae-BokNamb., 2014. Investigation of a new incremental counter forming in flexible roll forming to manufacture accurate profiles with variable cross-sections. International Journal of Machine Tools & Manufacture. 86. 68-80.

[6] M.M.Kasaei., H.Moslemi Naeini., R.Azizi Tafti., M.Salmani Tehrani., 2014. Prediction of maximum initial strip width in the cage roll forming process of ERW pipes using edge buckling criterion. Journal of Materials Processing Technology. 214. 190-199.

[7] M.M.Kasaei., H.Moslemi Naeini., B. Abbaszadeh, M. Mohammadi, M. Ghodsi, M. Kiuchi, R. Zolghadr, G. Liaghat, R.A. Tafti and M. S. Tehrani., 2014. Prediction of maximum initial strip width in the cage roll forming process of ERW pipes using edge buckling criterion. Journal of Materials Processing Technology. 214. 190-199.

[8] Tianxia Zou., Guanghan Wu., Dayong Li., Qiang Ren., Jiyuan Xin., Yinghong Peng., 2015. A Numerical method for predicting O-forming gap in UOE pipe manufacturing. International Journal of Mechanical Sciences. 98. 39-58.

[9] Tianxia Zou., Dayong Li., Guanghan Wu., Yinghong Peng., 2016. Yield strength development from high strength steel plate to UOE pipe. Materials Science and Engineering A. 551. 192-199.

[10] Qiang Ren., Tianxia Zou., Dayong Li., Ding Tang., Yinghong Peng., 2015. Numerical study on the X80 UOE pipe forming process. Journal of Materials Processing Technology. 215. 264-277.

[11] M.D.Herynk., S.Kyriakids., A.Onoufriou., H.D Yun., 2007. Effects of the UOE/UOC pipe manufacturing process on pipe collapse pressure. Materials and Design. 89. 1107-1122.

ACCEPTED MANUSCRIPT

[12] Q. Yin n., C. Soyarslan., A.G¨ uner., A.Brosius., A.E.Tekkaya., 2012. A cyclic twin bridge shear test for the identification of kinematic hardening parameters. International Journal of Mechanical Sciences.59,31-43.

[13] Jun Chen., Yuzhong Xiao., Wei Ding., Xinhai Zhub., 2015. Describing the non saturating cyclic hardening behavior with a newly developed kinematic hardening model and its application in springback prediction of DP sheet metals.215.151-158.

[14] Fusahito Yoshida., Takeshi Uemori., Kenji Fujiwara., 2002. Elastic–plastic behavior of steel sheets under in-plane cyclic tension–compression at large strain. International Journal of Plasticity. 18. 661-686.

[15] Fusahito Yoshida., Takeshi Uemori., 2003. A model of large strain cyclic plasticity describing the Bauschinger effect and workhardening stagnation. International Journal of Mechanical Science.45, 1687-1702.

[16] Liang-Jiu Jia., 2014. Integration algorithm for a modified Yoshida–Uemori model to simulate cyclic plasticity in extremely large plastic strain ranges up to fracture. Computers and Structures.145.36-46.

[17] Abbas Ghaei., AboozarTaherizadeh., 2015. A two surface hardening plasticity model based on non associated flow rule for anisotropic metals subjected to cyclic loading. International Journal of Mechanical Sciences.92,24-34.

[18] Satosh Sumikawa., Akinobu Ishiwatari., Jiro Hiramoto.,Toshiaki Urabe, 2014. Improvement of Springback Prediction Accuration Using Material Model Consideriong Elastoplastic Anisotropy and Bauschinger Effect. Journal of the JSTP. 55. 949-953.

[19] Liang-Jiu Jia, Hitoshi Kuwamura, 2015. Ductile fracture model for structural steel under cyclic large strain loading. Journal of Constructional Steel Research.106.110-221.

[20] E. Silvestre., J. Mendiguren., L.Galdos., E.Sáenz de Argandoña., 2015. Comparison of the hardening behaviour of different steel families : From mild and stainless steel to advanced high strength steels. International Journal of Mechanical Sciences. 101-102. 10-20.

[21] Frederic Barlat, Jose J. Gracio, Myoung-Gyu Lee, Edgar F. Rauch, Gabriela Vincze, 2011 An alternative to kinematioc hardening in classical plasticity. . International Journal of Plasticity. 27. 1309-1327.

[22] Yuzhong Xiao, Jun Chen, Jian Cao, 2012 A generalized thermodynamic approaches for modeling nonlinear hardening behaviors. International Journal of Plasticity. 38. 102-122.

[23] Lucia G. Barbu., Xavier Martinez., Sergio Oller., Alex H. Barbat., 2015. Validation on large scale tests of a new hardening–softening law for the Barcelona plastic damage model. International Journal of Fatigue. 81. 213-226.

[24] Seung Yooub Han, Seok Su Sohn, Sang Yong Shin, Jin-ho Bae, Hyoung Seop Kim, Sunghak Lee, 2012. Effects of microstructure and yield ratio on strain hardening and Bauschinger effect in two API X80 linepipe steels. Materials Science and Engineering A. 551. 192-199.

[25] Seok Su Sohn, Seung Yooub Han, Jin-ho Bae, Hyoung Seop Kim, Sunghak Lee, 2013. Effects of microstructure and pipe forming strain on yield strength before and after spiral pipe forming of API X70 and X80 linepipe steel sheets. Materials Science and Engineering A. 573. 18-26.

[26] M. Zeinoddini, M. Ezzati, G.A.R Parke, 2015. Plastic buckling, wrinkling and collapse behavior of dented X80 steel line pipes under axial compression. Journal of Loss Prevention in the Process Industries.38. 67-78.

[27] Frank F.Kraft., Tommy L.Jamison., 2012. Mechanical Behavior of Internally pressurized Copper Tube for New HVACR Applications. Journal of Pressure Vessel Technology. 134. 161213_1-161213_9

ACCEPTED MANUSCRIPT

[28] Fabrice Morestin, and Maurice Boivin, 1996. On the necessity of taking into account the variation in the Young modulus with plastic strain in elastic-plastic software. Nuclear Engineering and Design, 162, 107-116.

[29] Hong, G. J., Kim, M. S., Choe, D. H., 2000. Progressive quadratic approximation method for effective constructing the second-order response surface models in the large scaled system design. Transactions of the Korean Society of Mechanical Engineers A, 24(12), 3040-3052.

[30] Gehring, A., Saal, H., 2007. Yield strength distribution in thin-walled sections due to roll forming - a Finite-Element analysis, Proceedings of the 6th International Conference on Steel and Aluminum Structures, Oxford

[31] Gehring, A., Saal, H., 2007. Sensitivity analysis of technological and material parameters in roll forming, Proceedings of the 9th International Conference on Numerical Methods in Industrial Forming Processes, Porto

[32] Zou, T., Zhou, N., Peng Y., Tang, D., Li, D., 2016. Numerical Simulation of the Roll Forming Process of Aluminum Folded Micro-channel Tube, Journal of Physics: Conference Series 734. 032016.

[33] Tajyar, A., Abrinia, K., 2009. FEM Simulation of Reshaping of Thick Tubes in different passes, International Journal of Recent Trends in Engineering, 1:5, 82-85.

[34] Cai, Z., Wang, M., Li, M., 2014. Study on the continuous roll forming process of swept surface sheet metal part, Journal of Materials Processing Technology, 214, 1820-1827.

[35] Yang, H., Guo, L., Zhan, M., Sun, Z., 2006. Research on the influence of material properties on cold ring rolling processes by 3D-FE numerical simulation, Journal of Materials Processing Technology, 177, 634-638.

[36] Guo, L., Yang, H., 2006. Effect of sizes of forming rolls on cold ring rolling by 3D-FE numerical simulation, Trans. Nonferrous Met. SOC. China 16, s645-s651.

ACCEPTED MANUSCRIPT

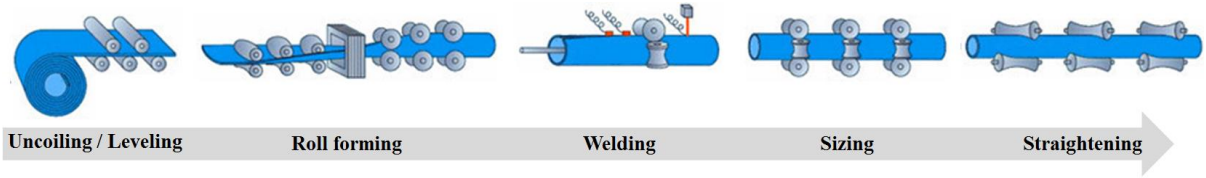

Fig. 1 Procedures of ERW roll forming process.

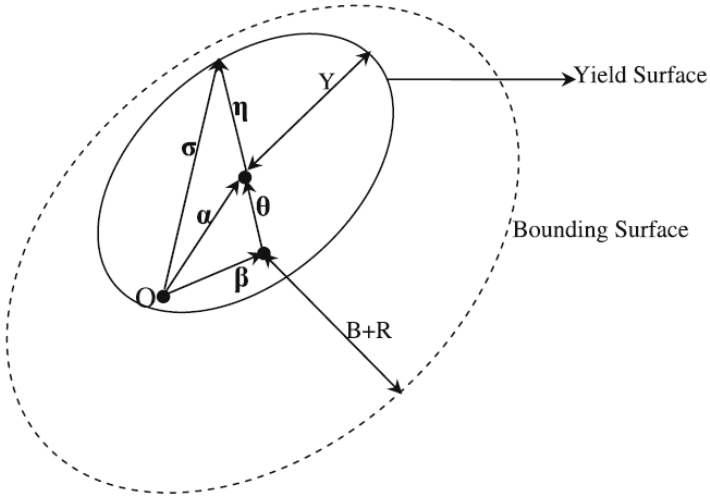

Fig. 2 Schematic illustration of the two-surface model [14]

ACCEPTED MANUSCRIPT

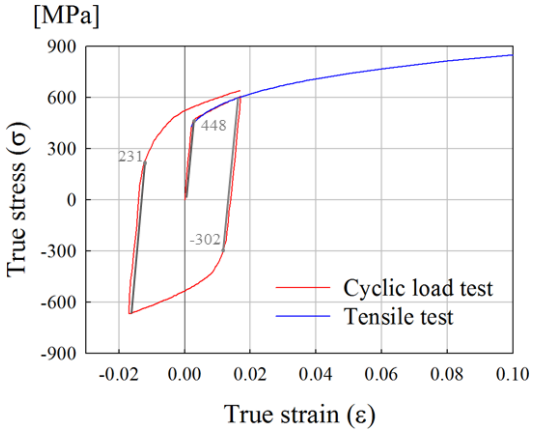

Fig. 3 Stress-strain curves from tensile test and cyclic load test of K55 material

ACCEPTED MANUSCRIPT

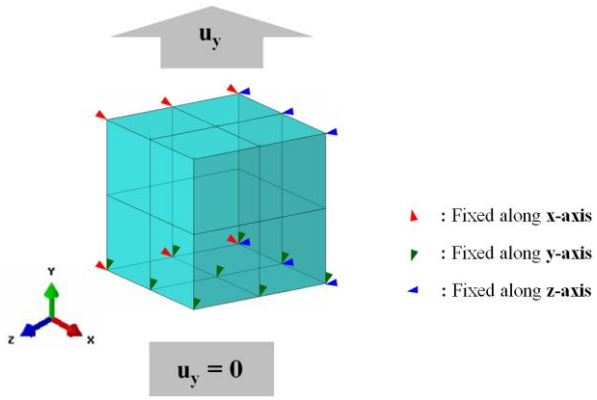

Fig. 4 Simple-element model to obtain model parameters

ACCEPTED MANUSCRIPT

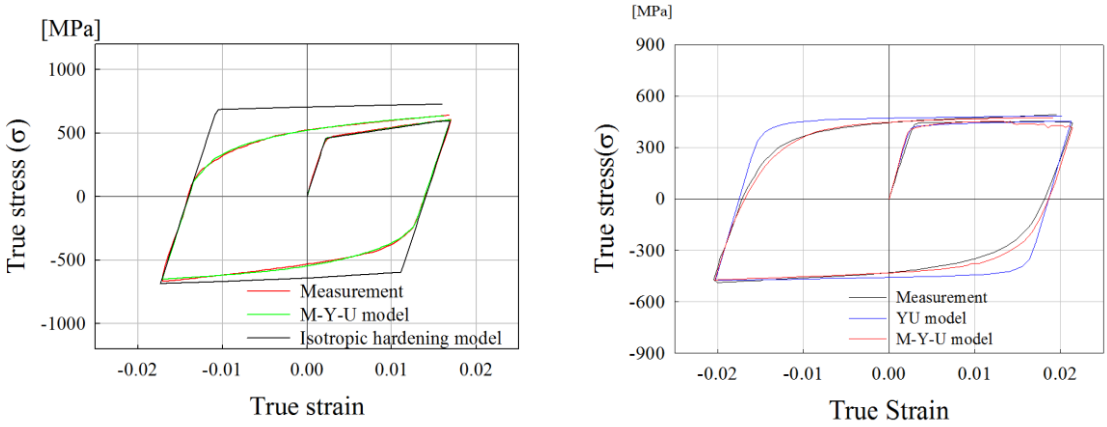

Fig. 5 True stress-strain curves under tension-compression cyclic loading

ACCEPTED MANUSCRIPT

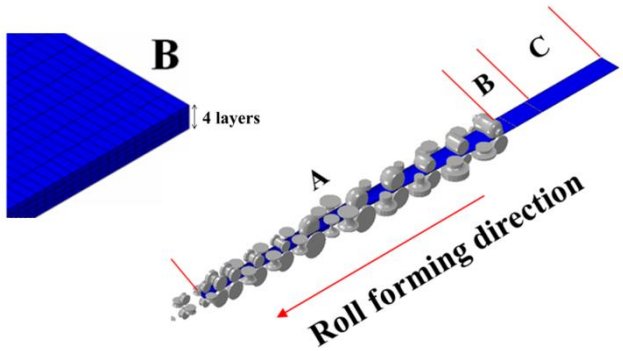

(a) Mesh sections in the roll forming simulation

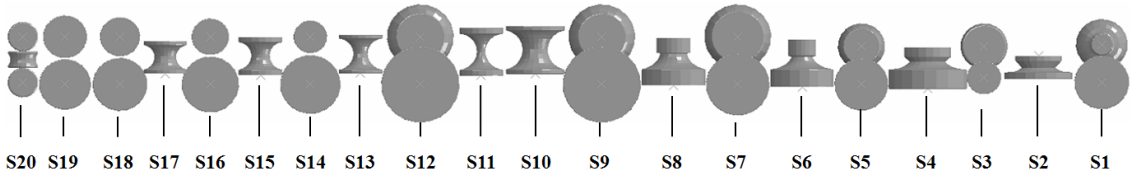

(b) Layout of roll stands

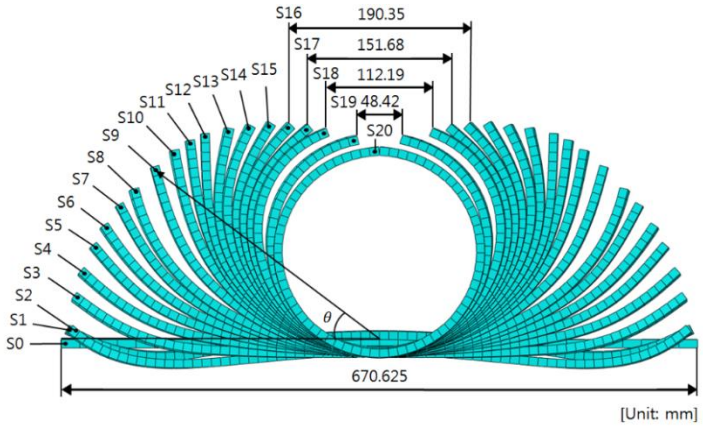

(c) The flower pattern of the roll forming process

Fig. 6 Schematic illustration of W-bending ERW pipe forming mill

ACCEPTED MANUSCRIPT

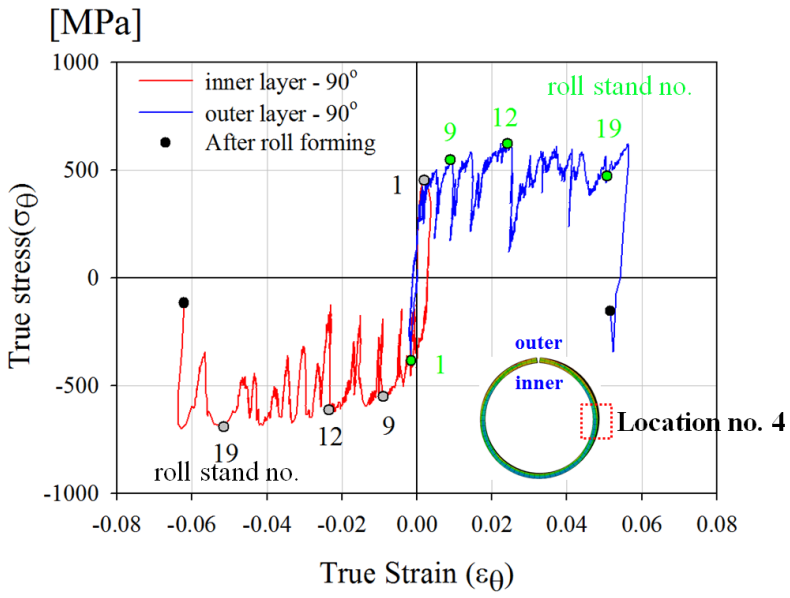

(a) At the 90 º -location from the weld line

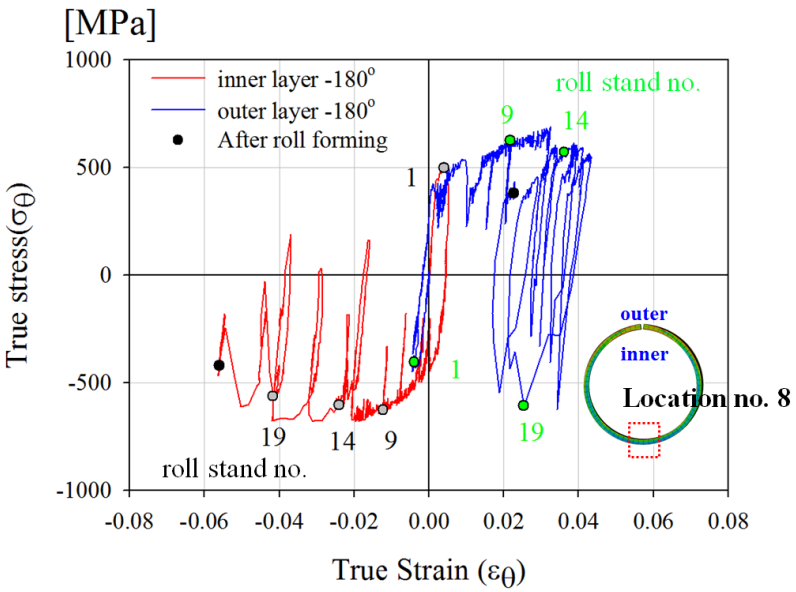

(b) At the 180°-location from the weld line

Fig. 7 Stress-strain history curve during roll forming process

ACCEPTED MANUSCRIPT

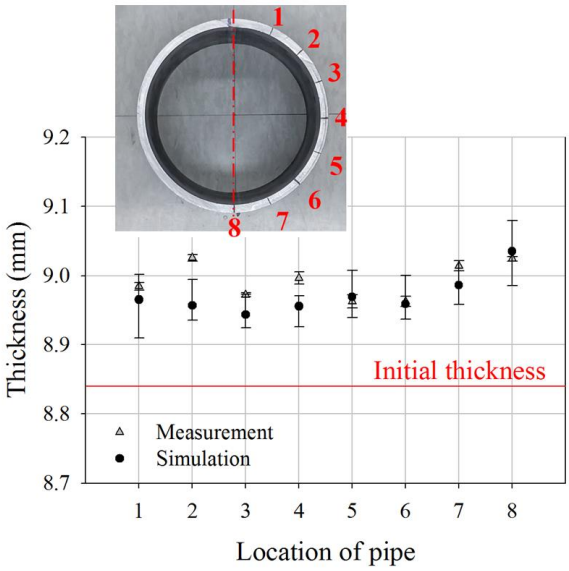

Fig. 8 Thickness distribution after sizing process with initial strip thickness of 8.84mm (sizing ratio 0.2%)

ACCEPTED MANUSCRIPT

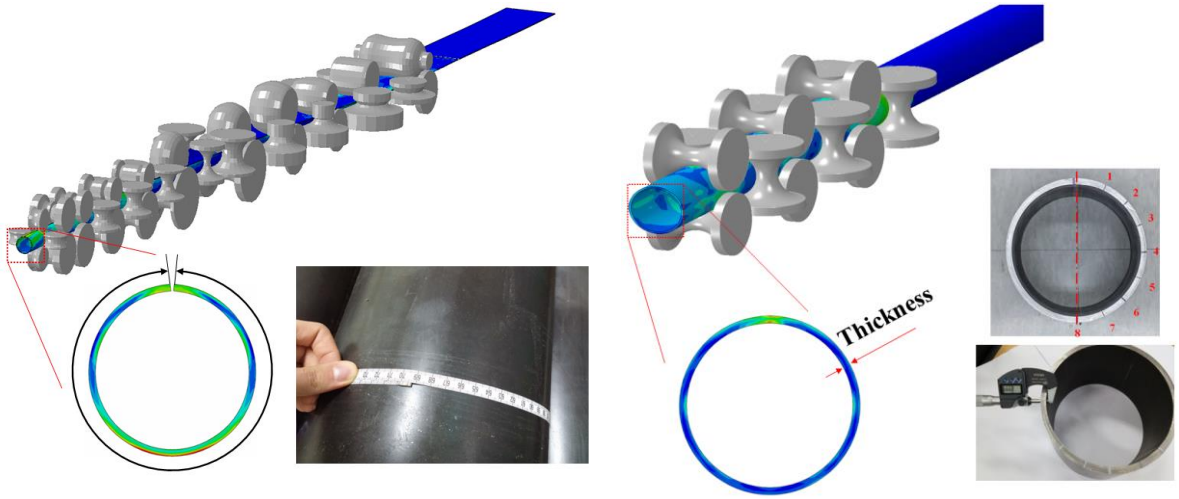

(a) Measuring the circumference length of pipe (b) Measuring the thickness of pipe

Fig 9. Measurement and simulation of the roll-formed ERW pipe

ACCEPTED MANUSCRIPT

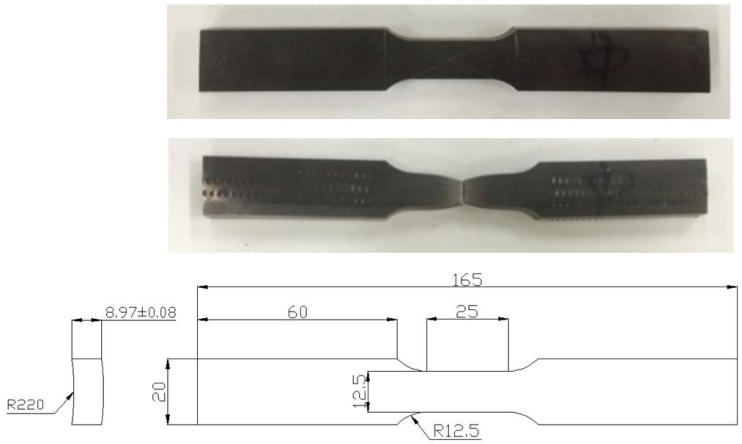

Fig. 10 Tensile specimens of pipe in the longitudinal direction

ACCEPTED MANUSCRIPT

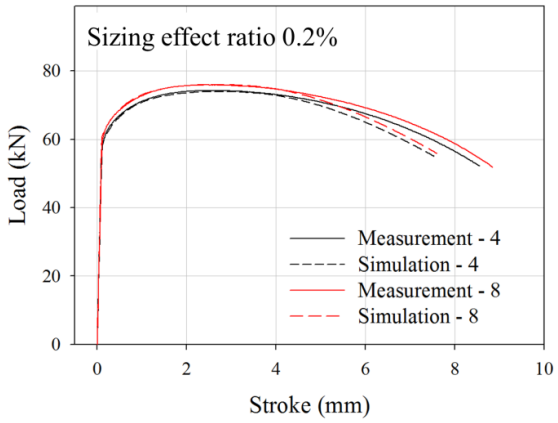

Fig. 11 load-stroke graph from pipe at pipe location #4 and #8

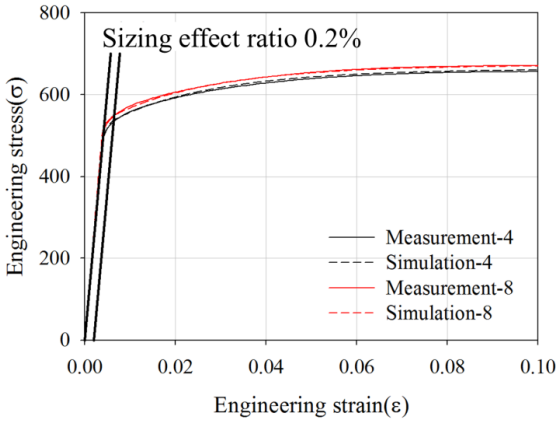

Fig. 12 Yield stress calculation in engineering stress-strain graph at pipe location #4 and #8

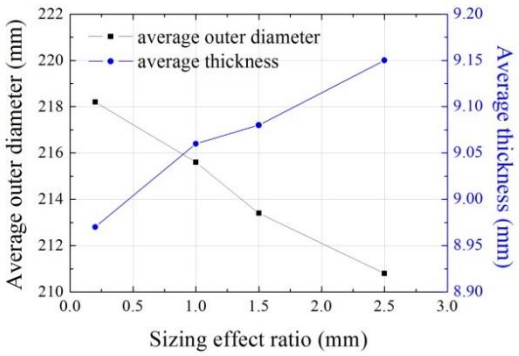

Fig. 13 The thickness and the diameter vs. the sizing effect ratio

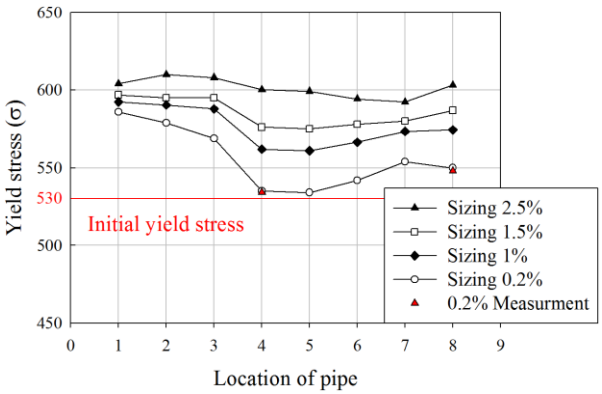

Fig. 14 The yield stress distributions along the circumferential direction

ACCEPTED MANUSCRIPT

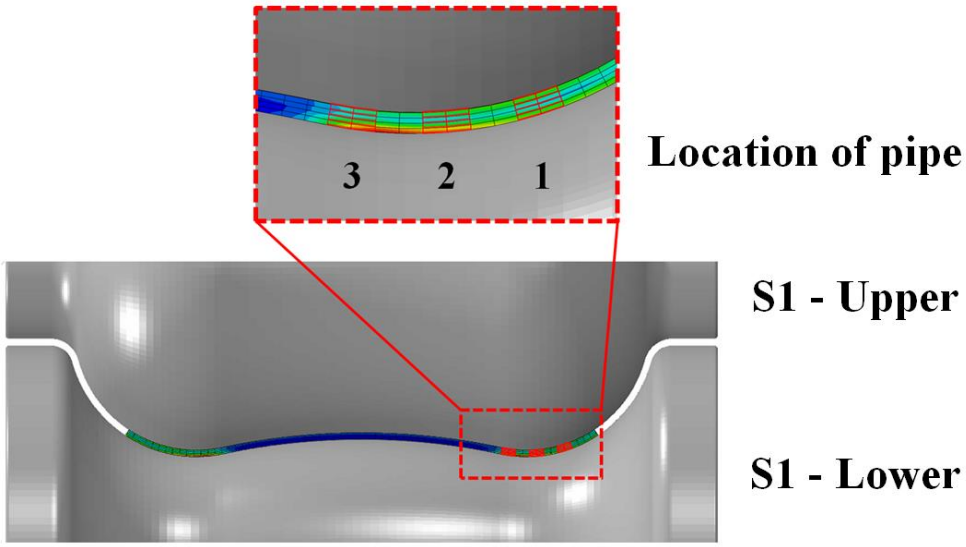

Fig. 15 Excessive deformation occurred in S1-stand

ACCEPTED MANUSCRIPT

Table 1 Chemical composition of K55 steel

Steel	**C**	**Si**	**Mn**	**Cr**	**P**
API K55	0.37	0.27	1.4	≤0.15	≤0.02

Table 2 Model parameters in the Modified Yoshida-Uemori model.

Parameters		**Parameters**		**Parameters**	
E_0 (GPa)	206	B_1 (MPa)	457	b_1 (MPa)	106
E_i (GPa)	180	B_2 (MPa)	397	b_2 (MPa)	244
x_i	15	B_3 (MPa)	340	b_3 (MPa)	261
$\sigma_{Y,1}$ (MPa)	453	$R_{sat,1}$ (MPa)	143	m_1	87
$\sigma_{Y,2}$ (MPa)	391	$R_{sat,2}$ (MPa)	255	m_2	35
$\sigma_{Y,3}$ (MPa)	347	$R_{sat,3}$ (MPa)	155	m_3	34
$\bar{\varepsilon}_1^p$	0.015	$\bar{\varepsilon}_2^p$	0.042	h	0.35
				C (MPa)	400

ACCEPTED MANUSCRIPT

Table 3 The simulation conditions of roll forming of a pipe.

Initial condition		**Fine mesh condition (section-B)**	
Number of roll pass	20	Mesh size in the longitudinal direction (mm)	4
Initial thickness (mm)	8.84	The number of mesh layers in the Thickness direction	4
Initial width (mm)	680	Total number of elements	72000
Coulomb friction coefficient	0.2	Mesh type	Hexahedron type C3D8R

Table 4 Bending increment per pass

Stand number	**Strip end-point angle [°]**	**Stand number**	**Strip end-point angle [°]**	**Stand number**	**Strip end-point angle [°]**
0	0	7	28.11	14	59.59
1	2.65	8	32.22	15	64.03
2	2.75	9	38.27	16	68.12
3	8.85	10	43.50	17	72.32
4	13.72	11	47.22	18	76.13
5	18.97	12	50.47	19	84.07
6	23.24	13	55.33	20	89.99

Table 5 - Circumference length of pipe before and after welding

Circumference length	Measurement [mm]	Simulation [mm]
After roll forming (before welding)	691	691 (mean value)
Before Sizing(after welding)	689	689 (mean value)